Determination of dissolved nickel in natural waters using a rapid microplate fluorescence assay method

Fabien Robert-Peillard, El Mountassir El Mouchtari, Damien Bonne, Stéphane Humbel, Jean-Luc Boudenne, Bruno Coulomb

Determination of dissolved nickel in natural waters using a rapid microplate fluorescence assay method

Fabien Robert-Peillard[1], El Mountassir El Mouchtari[1], Damien Bonne[2], Stéphane Humbel[2], Jean-Luc Boudenne[1], Bruno Coulomb[1*]

[1]Aix Marseille Univ, CNRS, LCE, Marseille, France

[2]Aix Marseille Université, CNRS, Centrale Marseille iSm2, Marseille, France

[*]Corresponding author: bruno.coulomb@univ-amu.fr

Abstract

A new microplate analytical procedure is described for the determination of nickel (Ni^{2+}) ions in natural water samples. A lophine analogue fluorescent sensor was synthesized and a spectral study showed a selective fluorescence quenching effect of chemical sensor by Ni^{2+} under optimized conditions. Density functional theory (DFT) calculations confirmed the formation of a $Ni(II)L_3$ complex obtained by the Job plot. The calculations showed that the fluorescence emission peak of L collapses due to the distortion of L in the complex. The simple and fast microplate procedure allowed us to quantify Ni^{2+} with a linear response from 1.6 to 40 µg L^{-1} and a quantification limit of 5.4 µg L^{-1} without the need of a preconcentration step. The optimized procedure using high-throughput microplate assay has been applied for the determination of Ni^{2+} in natural water samples with good analytical performances.

Keywords:

Fluorescent chemical sensor; nickel; lophine derivative; high-throughput analysis; natural waters

1. Introduction

Nickel is naturally present in small quantities in the earth's crust (about 0.02%), mainly in the form of sulfide, oxidized and silicate ores, and has a very important role in various enzymatic activities of some plant and bacterial enzymes. However, nickel is widely used in many industrial sectors such as electroplating, battery or painting industries leading to releases into the aquatic environment. Nickel can become harmful to the environment, causing pollution of water and soil, and orally ingested nickel may have adverse effects on kidneys and lungs and can promote the development of dermatitis, eczema, respiratory diseases or even cancer [1,2].

For the environment, the European Community has established an annual average value of environmental quality standard (AA-EQS) of 4 µg L^{-1} for inland surface water and a maximum allowable concentration value of environmental quality standard (MAC-EQS) of 34 µg L^{-1} irrespective of the kind of water bodies. The presumed carcinogenicity of nickel and its compounds have led the health authorities to establish limit values in water intended for human consumption, to limit human exposure. In Europe, this limit has been set at 20 µg L^{-1} while the World Health Organization (WHO) recommends a maximum guideline value of 70 µg L^{-1}.

In laboratory, nickel is typically quantified by several analytical techniques including inductively coupled plasma-atomic emission spectrometry (ICP-AES), inductively coupled plasma-mass spectrometry (ICP-MS) and graphite furnace atomic absorption spectrometry (GF-AAS) or flame atomic absorption spectrometry (F-AAS). The analytical performance of these methods can be improved by sample processing steps such as liquid-liquid extraction [3] or solid-phase extraction [4,5], to pre-concentrate the analyte and facilitate its detection or to limit interference from sample matrix. These techniques however often require expensive equipment and complex and time-consuming analytical procedures.

These disadvantages have led researchers to develop in recent years more sustainable chemical techniques, to reduce the cost and environmental impact of the analyses. This can be achieved by reducing the volumes used (principles 1 and 2 of green chemistry: waste prevention and atoms economy, respectively) and energy consumption (principle 6: design for energy efficiency), or even by real-time monitoring with a view to preventing pollution (principle 11: real-time analysis for pollution prevention). To achieve these objectives, the use of microplates is advantageous, thus taking advantage of low consumption of samples and reagents, possibilities of automation, rapid preparation, and multisampling analyses. However, the development of such a microplate method requires the use of a sensitive and selective chemical probe allowing spectrophotometric or fluorescence detection.

Spectroscopic techniques (UV-visible spectrophotometry or fluorescence) are of great interest due to their robustness, low cost, and ease of use, but they often suffer from interference from transition metals, especially Fe (II), Co (II), Cu (II), Pb (II) and Zn (II) [6] and from high quantification limits which prevent their use for environmental analyses. To overcome these problems, three ways have been considered in recent years: the development of extraction/pre-concentration processes, the use of chemometrics and the synthesis of selective chemical probes.

Solid-phase extraction has been applied by Mizuguchi et al. [7] and by Liu et al. [8], respectively using a Nylon 6 membrane and Amberlite XAD-4 resin beads, to preconcentrate nickel as a metal complex and perform the detection by solid-phase spectrophotometry. Likewise, Adewuyi et al. [9] have proposed an analytical method based on the pre-concentration of nickel on nanofibers of poly-(acrylic acid) functionalized with pyridilazo-2-naphthol and followed by fluorescence detection. Concerning chemometrics, overlapping peaks of UV-visible spectra of interferent metal complexes for nickel determination has been solved by derivative spectroscopy [6], Partial Least Squares calibration [10,11] or light-absorption ratio variation approach (LARVA) [12]. However, solid-phase extraction procedures or exploitation of UV-visible spectra are difficult to apply to microplate analyses.

Some studies have also focused on the synthesis of various chemical sensors for the selective complexation of nickel, but in 2012 only 6% of studies on synthesis of chemical probes concerned the determination of nickel [13] and few of them had been applied to nickel analysis in real water samples. We can cite for example Chowdhury et al. [14] and Wang et al. [15] who have respectively synthesized a Schiff base and an acridine based fluorescent chemosensors for selective nickel determination by chelation-enhanced fluorescence. In the same way, a hydrazide compound was synthetized by Liu et al. [16] and was applied to direct nickel determination of nickel in river water samples.

Table 1 presents a comparison of various spectroscopic methods (UV-Vis spectrophotometry or fluorescence) applied to nickel quantification in tap water, natural waters (river water, lake water, groundwater) or in wastewater. Data analysis of this table shows that few methods are available and applicable, particularly considering the whole operational parameters required for quantification of nickel in natural or drinking water (ease of use, duration, limit of quantification, selectivity),. Some of these methods are extremely sensitive with satisfactory detection limits for the analysis of nickel in drinking or natural water but are either complex and long to implement [7,8,11,12,17], or not sufficiently selective for environmental matrices [9]. The other methods do not have a detection limit low enough to be applied to the analysis of drinking water according to European regulations: for water sanitary control, an analytical method must be capable of measuring concentrations equal to 30% of the parametric value with an uncertainty of measurement of 25%, i.e. for nickel determination, this corresponds to a limit of quantification of 6 µg L^{-1} and a limit of detection of approximately 2 µg L^{-1} [24].
The development of a rapid, sensitive, and selective determination of nickel in water samples is therefore still a challenge. Ideally this method should be robust, low cost and with simple operational conditions so that it can be easily applied to various environmental matrices.
In this paper we report the synthesis of a new fluorescent chemosensor **L** (4-[4,5-di(pyridin-2-yl)-1H-imidazol-2-yl]benzoic acid). This chemical sensor **L** can be considered as an analogue of lophine (2,4,5-triphenylimidazole) and lophine and its derivatives are known to be highly fluorescent and have already been reported as chemiluminescence compounds using hydrogen peroxide [25,26] or for determination of trace amounts of cobalt [27]. In this study, we investigated sensing possibilities of sensor **L** towards metal ions and optimized analytical parameters of a rapid, direct, and simple microplate procedure to reach low detection limit. This procedure was applied to selective nickel detection in drinking and natural water samples.

1 **Table 1** : Comparison of analytical features of spectroscopic techniques for nickel determination in environmental water samples

Method	Ligand or sensor	Matrix	Linear range (µg L^{-1})	Detection limit (µg L^{-1})	Quantification limit (µg L^{-1})	Analytical procedure duration (min)	Main tolerance limit (molar ratio relative to Ni^{2+})	Reference
Spectrophotometry	DSPCF[a]	River water, wastewater	5 - 200	1.3	n.d.	> 15	Fe^{2+} : 10 Mn^{2+} : 10	[12]
Fluorescence	BMH[b]	River water	4.7 - 117	3.5	n.d.	< 1	Co^{2+} : 1 Mg^{2+} : 2	[16]
Solid phase spectrophotometry	o-CDAA[c]	Tap water	0.48 - 25	0.14	0.48	> 20	Co^{2+} : 1	[8]
Spectrophotometry	azocalix[4]arene[d]	Drinking water	10 - 299	8.2	n.d.	< 1	Co^{2+} : 3 Cu^{2+} : 3	[18]
Solid phase spectrophotometry	α-furil dioxime	Rainfall water	1 - 12	0.7	n.d.	> 15	Cu^{2+} : 10 Co^{2+} : 100	[7]
Solid phase fluorescence	Pyridylazo-2-naphthol	Water Certified Reference Material	100 - 1000	0.07	n.d.	< 1	Co^{2+} : 1 Fe^{2+} : 1	[9]
Fluorescence	Schiff base[e]	Water	100 - 1200	99	n.d.	< 1	Cu^{2+} : 1	[19]
Spectrophotometry	Xylenol orange	Water	1 - 5000	0.13	n.d.	> 13	n.d.	[11]
Fluorescence	Schiff base	Tap water, river water	50 - 1700	50	n.d.	< 1	Hg interference	[20]
Fluorescence	Murexide	Groundwater, seawater, rainwater	7 - 100	4	n.d.	< 1	Co^{2+} : 5 Cu^{2+} : 5	[21]

Spectrophotometry	GSH-AgNPR[f]	Tap water, lake water	0.3 - 17	0.3	n.d.	> 15	Co interference	[17]
Spectrophotometry	dimethylglyoxime	River water, wastewater	50 - 600	20	n.d.	n.d.	Cu^{2+} : 10 Co^{2+} : 100	[22]
Fluorescence	BNQDs[g]	River water, lake water	5.9 - 5900	5.9	n.d.	> 5	Some interferences	[23]
Microplate fluorescence	L	Natural water ; Groundwater	1.6 - 40	1.6	5.4	< 1	Cu^{2+} : 92[h]	This work

n.d. : not determined

[a] 1,5-di(2-hydroxy-5-sulfophenyl)-3-cyanoformazan ; [b] N'-(1,3 dimethylbutylene)-3-hydroxy-naphthohydrazide ; [c] o-carboxylphenyldiazoaminoazobenzene ; [d] 5,17-bis(quinolyl-8-azo)-25,26,27,28-tetrahydroxycalix[4]arene ; [e] N'-(2-hydroxy-3-methoxybenzylidene)-2-(benzamido)benzohydrazide ; [f] silver nanoprisms (AgNPRs) stabilized with glutathione (GSH) ; [g] boron nitride quantum dots; [h] in presence of thioglycolic acid as masking agent.

2. Experimental

2.1. Chemicals and reagents

All reagents and solvents used were of analytical grade. Aqueous solutions were prepared with ultrapure deionized water using a Millipore Milli-Q purification system (Millipore, USA, resistivity > 18 MΩ cm). A 0.1 M phosphate buffer solution was prepared by dissolving appropriate amount of potassium dihydrogen phosphate (Merck, Germany) in ultrapure water and adjusted to pH = 7 by adding a few drops of 1 M NaOH solution.
10 mM stock solution of 4-[4,5-di(pyridin-2-yl)-1H-imidazol-2-yl]benzoic acid (sensor **L**) was prepared in dimethylsulfoxide (DMSO) and stored at +4 ◦C. This stock solution was then diluted in phosphate buffer to give 10 µM working solution.
Ni^{2+} and interferents (Ag^{+}, Al^{3+}, Ca^{2+}, Cd^{2+}, Co^{2+}, Cr^{3+}, Cu^{2+}, Fe^{3+}, Hg^{2+}, Mg^{2+}, Mn^{2+}, Pb^{2+}, Pt^{4+}, Ti^{3+}, Zn^{2+}) standards were prepared daily by dilution of 1 g L^{-1} commercial standards solutions (AAS solution 1 mg mL^{-1} Acros Organics, France) with ultrapure water.
A 10 mM masking agent stock solution was prepared by diluting commercial thioglycolic acid (Acros Organics, France) in phosphate buffer solution. This stock solution was then diluted daily in phosphate buffer to give the working solutions.

2.2. Synthesis and characterization of sensor **L**

The synthetic route reported by Slater et al. [28] was modified to introduce a carboxylate group in the structure of the sensor through formylbenzoic acid and improve water solubility. The synthesis of sensor **L** is briefly described hereafter (Scheme 1). 4-Formylbenzoic acid (0.50 g, 3.33 mmol, 1.0 equiv) was added to a solution of 2,2'-pyridil (0.71 g, 3.33 mmol, 1.0 equiv) and ammonium acetate (2.10 g, 27.2 mmol, 8.0 equiv) in acetic acid (10 mL). The mixture was heated in a microwave for 5 minutes at 180 °C. The reaction mixture was allowed to cool to room temperature and neutralized with ammonia solution in an ice bath. The pale-yellow precipitate formed was collected, washed with water, and recrystallized from acetone to afford the desired product as a light-yellow solid (0.35 g, 35% yield). **Mp** : 308 – 310 °C; **^{1}H NMR (400 MHz, DMSO-d_6) δ (ppm)** δ 9.91 (brs, 1H), 8.60 (d, *J* = 4.9 Hz, 2H), 8.30 (d, *J* = 8.1 Hz, 2H), 8.11 (d, *J* = 8.1 Hz, 2H), 8.03 (d, *J* = 8.1 Hz, 2H), 7.84 (td, *J* = 7.5, 2.0 Hz, 2H), 7.32 (dd, *J* = 7.5, 4.8 Hz, 2H); **^{13}C NMR (100 MHz, DMSO-d_6) δ (ppm) δ** 172.54, 168.12, 149.00, 145.84, 136.85, 133.56, 133.24, 130.01, 125.93, 123.61, 122.75 (Fig. S1); **HRMS-ESI^{+} (m/z)** : found $[M+H]^{+}$ 343.1186, calculated $C_{20}H_{15}N_4O_2$ requires 343.1190.

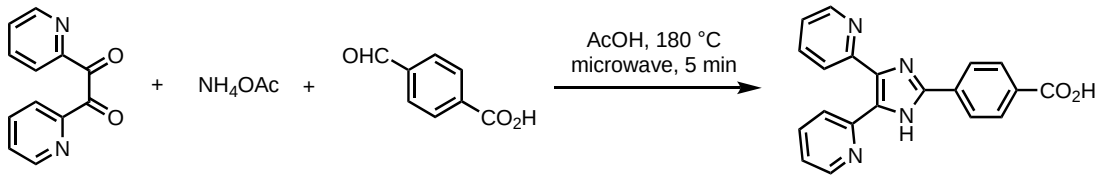

Scheme 1 : Synthetic route for 4-[4,5-di(pyridin-2-yl)-1H-imidazol-2-yl]benzoic acid (sensor **L**).

2.3 Fluorescence measurements

Fluorescence study of sensor **L** was carried out on a SAFAS Xenius fluorescence spectrometer (SAFAS, Monaco) equipped with a Xenon lamp and controlled by SP2000 V7 software. Sensor **L** and metal ion were mixed into a quartz cell following a ML_3 ratio and fluorescence spectrum of each mixture was measured using an excitation wavelength of 340 nm (excitation and emission bandpass: 10 nm; wavelength step: 1 nm; scan speed: 260 $nm.min^{-1}$; photomultiplier voltage: 600 V).

Microplate fluorescence was measured on a multi-mode microplate reader (Synergy HTX, Biotek, France), equipped with excitation and emission filter wheels and controlled by Gen5 version 3.03 software (Biotek). Top fluorescence detection was performed in polypropylene black 96-well U-bottom microplates (Nunc) from above the microplate wells, at λex = 340 nm and λem = 440 nm.

2.4 Computational study

The computed results correspond to single point calculations with the B3LYP DFT method [29-31] and the def2-TZVP [32,33] basis set on top of BP86 optimized geometries [34-36] with the def2-SVP basis set [32,33]. All the computations used the maximum symmetry group (C_3 for the $(NiL_3)^{2+}$ complexes, C_s for the isolated lophine). All structures were characterized as minimum with frequency calculation. The D3 dispersion correction was applied in all computations [37]. The Ni complex structures were dications at the triplet state. Counter anions were not considered. The Turbomole suite of program [38-40] was used throughout with the resolution of identity method [41-45]. The calculation levels were very similar to that of Dowling et al.[46].

The UV-Vis spectra of the lophines were computed at the B3LYP/def2-TZVP level within the TDDFT framework.[47]. For the planar lophine a total of 12 states were requested (8 of a' symmetry, and 4 of a"). For the lophine distorted as in the $Ni(II)L_3$ complex, 15 states were requested. A 9 states computation showed that the part of the spectrum that is low in energy is not sensitive to the number of states.

2.5 Microplate assay for Ni^{2+} determination

100 µL of sample or Ni^{2+} standard solution was dispensed into the wells of the microplate, followed by 100 µL of a 10 µM sensor **L** solution in phosphate buffer pH = 7 and 30 µL of masking agent solution. The plate was shaken for 20 sec in the microplate reader and fluorescence was subsequently measured at λex=340 nm and λem=440 nm. All experiments were performed in triplicate.

2.6 Validation on real samples

Groundwater samples were collected from sources and drillings used to produce water intended for human consumption, in the Aubagne region, near Marseille (Provence Alpes Côte d'Azur region, South-East of France). A river water sample was collected from the Huveaune River (Aubagne, France). A location map of the sampling points is provided in supplementary

materials (Fig. S2). Samples were filtered on-site using 0.45 µm polyether sulfone (PES) filters and stored in high density polyethylene flasks at +4 °C until analysis.

Samples were analyzed both by the developed microplate assay described above and by inductively coupled plasma mass spectrometry (ICP/MS; Agilent 7800, Agilent Technologies, France) controlled by Agilent MassHunter version 4.5 software for data acquisition and analysis. Instrumental settings were as follows: plasma energy, 1000 W; carrier gas, 12 L min^{-1}; makeup gas, 0.4 L min^{-1}. Instrument performance for elemental analysis was verified with a diluted of multi-element JYICP-MIX21 100 mg L^{-1} solution in 5% nitric acid (Jobin-Yvon, France).

2.7 Sustainability evaluation of the method

The greenness and the sustainability of the method were evaluated by the RGB_{12} model [48,49] and compared to similar methods for the detection of nickel in aqueous samples by spectrophotometry with an azocalix[4]arene [18], solid-phase spectrophotometry with o-CDAA [8], and fluorescence with BMH [16] or with murexide [21].
The RGB model allows the comparison of methods according to 12 rules divided into 3 components: the red component (principles R1-R4) for the evaluation of analytical performance and the green (principles G1-G4) and blue (principles B1-B4) components for the evaluation of the method's ecological and practical criteria respectively. The criteria used are detailed in Table S1. For each method, the evaluation was based on the analytical part of the method, the chemical probe synthesis steps were not considered. The criteria are evaluated individually and an overall score of the method is calculated in a range between 0 and 100, the closer the score is to 100 the more satisfactory the method is in terms of analytical performance, greenness, and sustainability.

3. Results and discussion.

3.1 Fluorescence study of **L** towards Ni^{2+}

The sensing possibilities of sensor **L** towards metal ions were first investigated by fluorescence spectra measurement in aqueous solutions. The carboxylate group introduced in the structure of the sensor through formylbenzoic acid helped to improve water solubility and enabled application in aqueous solutions. Excitation and emission wavelengths were determined by performing a 3D fluorescence scan of sensor **L** in phosphate buffer (Fig. S3). The results showed an excitation wavelength and an emission wavelength centered at 340 nm and 417 nm respectively, which is consistent with the wavelengths reported previously for lophine derivatives [26,50]. The fluorescence spectra of **L** with the presence of various metal ions were recorded and are shown in Fig. 1a. From these results, we can observe that sensor **L** exhibited a high fluorescence at 417 nm while fluorescence strongly decreased in the presence of Ni^{2+}. Fluorescence is also slightly decreased in the presence of Cu, Co and Hg while other metals tested do not appear to cause fluorescence quenching.

The stoichiometry of the complex between sensor **L** and Ni^{2+} was established using Job's plot analysis (Fig. 1b). The plot of fluorescence intensity versus molar ratio of **L** and Ni^{2+} showed a

maximum quenching effect of fluorescence around 0.25, which indicated a 3:1 stoichiometry between **L** and Ni^{2+}.

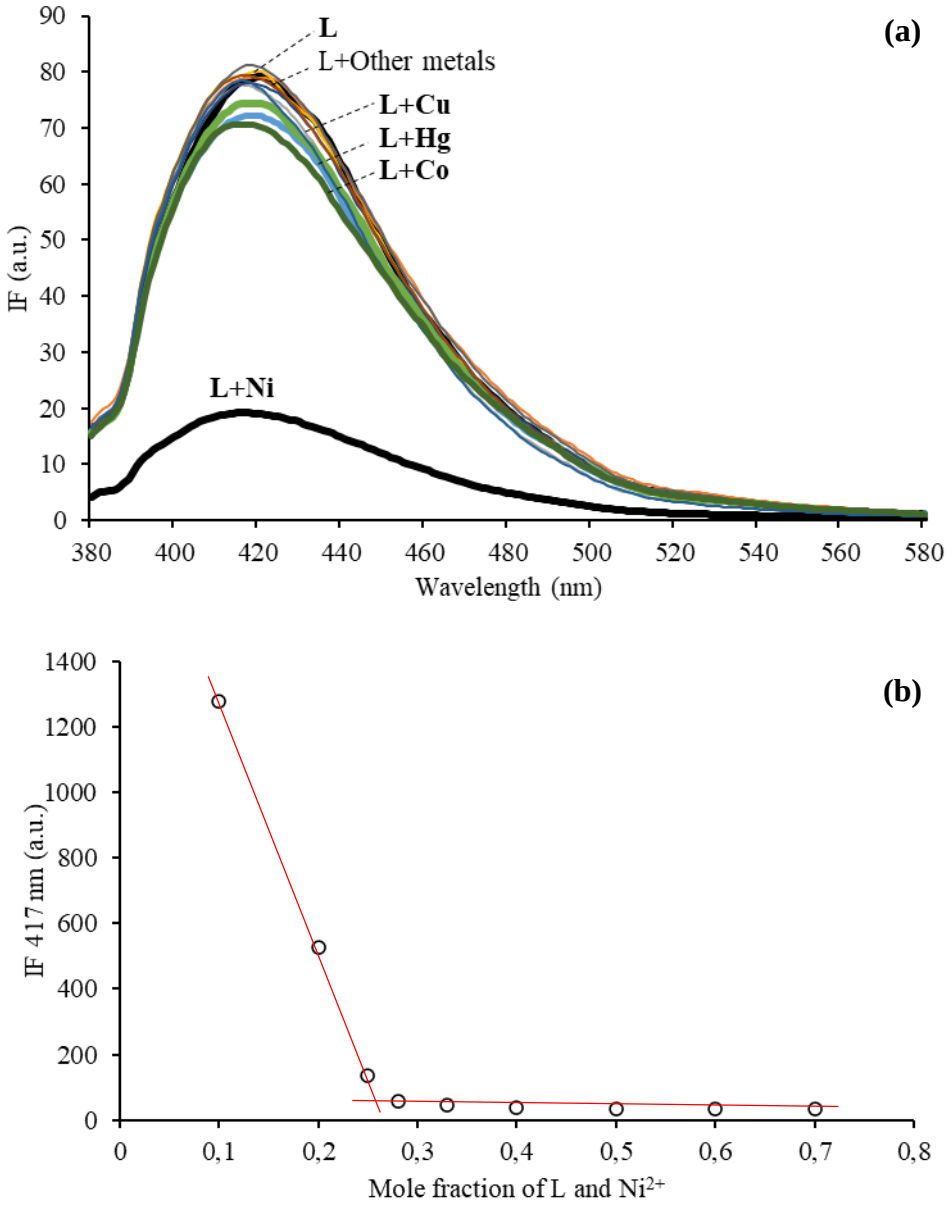

Figure 1: (a) Emission fluorescence spectra (λexc =340nm) of **L** (10 μM) in phosphate buffer (pH=7) and **L** with addition of various metal ions M (M:L_3 ratio); (b) Job's plot analysis of **L** (10 μM) regarding Ni^{2+} ion (10 μM).

3.2 $(NiL_3)^{2+}$ complexes

Our DFT computations converged to a stable C_3 symmetric structure, where each lophine interacts with the metal with η^2 coordination (Fig. 2). This structure is in agreement with the study of Dowling and Lemaire [46] in which an imidazole-based ligand complexed transition metals through bonds with the N atoms of pyridine and imidazole rings.

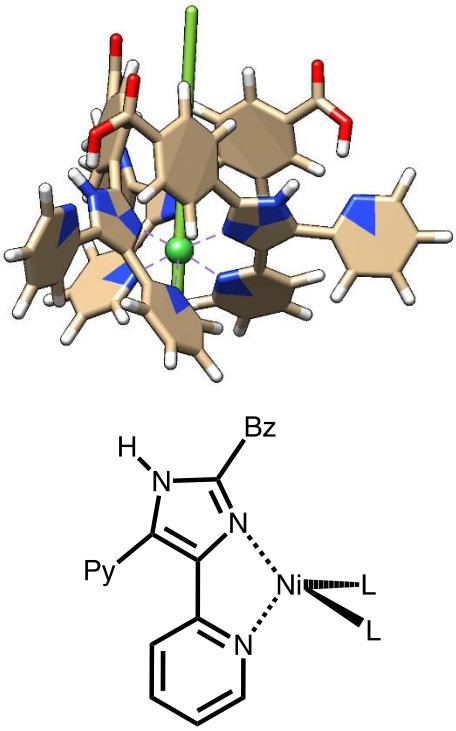

Figure 2: Possible complexation on Ni(II) with η2 coordination of each lophine. The green axis is the C_3 axis.

The π system of the lophines in the complexes is very different from that of a free lophine: (i) π systems of lophines see each other via π-stacking and/or CH-π interactions and (ii) the rings are partly deconjugated by rotations. Hence, it is not surprising that the π→ π* transition observed in free lophine is lost in the ML_3 complexes. The energy cost of the lophine's distortion can be as large as 119.8 kJ mol^{-1} (Fig. 3a).

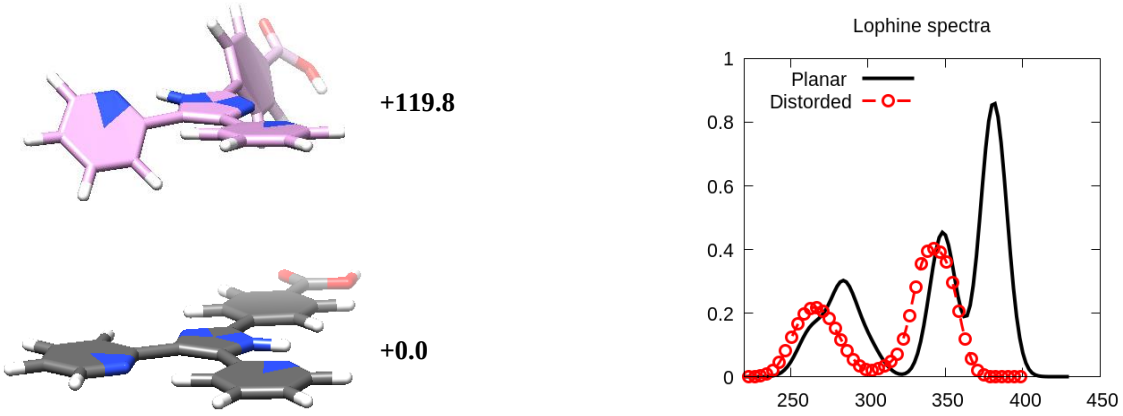

(a) **(b)**

Figure 3: Lophine distortion for the complexation on Ni(II) : (a) bottom free lophine, top as extracted from the η^2 complex. The number on the right is the energy destabilization with respect to a free lophine (bp86 def2-SVP values, in kJ mol^{-1}); (b) TD-DFT simulated spectrum.

Moreover, the simulated UV spectrum shows that the quenching effect can be at least partly attributed to this lophine's distortion (Fig. 3b). The computed free lophine shows 2 bands at 350 nm and 385 nm (Fig. 3b, plain black). The massive band observed experimentally at 417 nm must correspond to the coalescence of these two bands, with a large contribution of the most intense peak, at 385 nm. Hence, the computed spectrum is blue shifted by about 30-40 nm. In the distorted lophine the computations show that the most intense peak at 385 nm collapses, and the peak at 350 nm was the only one to remain. Hence, we attribute the fluorescence quenching, at least partly, to the distortion of the lophine in the complex. As stated above, π stacking effects in the complex shall also contribute to the quenching.

3.3. Optimization of the analytical protocol

3.3.1 pH and buffer solution

pH of the reaction mixture between **L** and a metal solution plays an important role because it can modify the characteristics of the functional coordination groups. A judicious choice of pH can allow both to obtain the best response for the determination of Ni^{2+} but also to limit interference from other metal elements. The effect of pH value was investigated here in the range 5 to 9 by addition of few drops of HNO_3 or NaOH diluted solutions (Fig. 4).

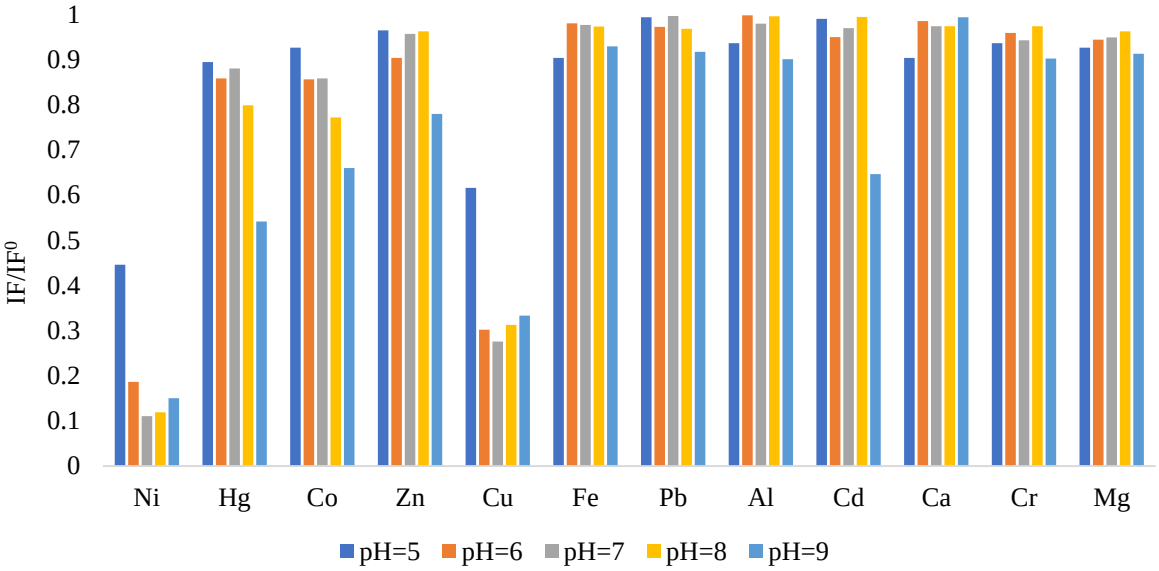

Figure 4: Fluorescence intensity ratio (IF/IF_0 is the ratio between the fluorescence response of the metal ions solution and the blank) as a function of pH (**L** at 10 µM and metal ions at 1 µM).

From Fig. 4, we can observe that the nickel response (quenching effect) was maximal and stable for pH values between 6 and 9. Most metals partially quenched the fluorescence of L for a pH value equals to 8 (Hg, Co, Cu) or 9 (Cd, Zn). Finally, the best compromise between the response of nickel and the response of interfering metals seemed to be at a pH equal to 7 because this

value could limit the interference of Hg, Co, and Zn. Only copper displays a similar profile as nickel, complexation by **L** appeared rather independent of pH between 6 and 9.
Two buffers at pH=7 were tested: a phosphate buffer and a HEPES buffer (4-(2-hydroxyethyl)-1-piperazineethanesulfonic acid). During the experiments, the phosphate buffer showed a slight increase in the IF_{metal}/IF_{blank} fluorescence ratio compared to the HEPES buffer for cobalt and mercury, making it possible to limit their possible interferences. The phosphate buffer at pH=7 was therefore chosen for subsequent experiments, but the results also showed that the interferences of copper, and to a lesser extent of cobalt and mercury, will have to be considered and eliminated by the addition of a masking agent.

3.3.2 Selectivity towards Ni and masking agent

The selectivity of a chemical probe for a metal ion is a paramount parameter for measurements in environmental samples. This is particularly important for metal ions whose environmental concentrations are in the range of µM (Ni^{2+}, Cu^{2+}, Zn^{2+}) while other metal ions could be present at levels of mM (Ca^{2+}, Mg^{2+}). In most publications, the selectivity study is carried out with the metal of interest in the presence of 1 to 10 equivalents of other metal ions, but for some metal elements these concentration levels are not representative of real environmental amounts. For this study, we set the Ni^{2+} concentration at 10 µg L^{-1} (0.17 µM) and the concentrations of interfering metal ions were based on parametric values defined by European legislation on water intended for human consumption (Cu^{2+}, Pb^{2+}, Cd^{2+}) or based on environmental values encountered in surface waters (Ca^{2+}, Mg^{2+}, Zn^{2+}). The response was studied with each metal ion separately at environmental level in absence and in presence of masking agent (Fig. 5). The selectivity study clearly demonstrated the strong interference of copper in the absence of a masking agent. The other metals at environmental levels showed no interference problems. Various masking agents have thus been tested to eliminate interference from copper with no masking of the response of nickel: tetraethylenepentamine (TETREN), triethanolamine (TEA), thiourea, thioglycolic acid, diethyldithiocarbamate (DDTC) [51]. TETREN, TEA and thiourea were shown to be not effective in masking interference from copper. DDTC eliminated the interference from copper but also masked the response of nickel. Finally, thioglycolic acid was found to be the most effective masking agent, helping to eliminate interference from other metallic elements at environmental concentrations (Fig. 5a). The concentration of thioglycolic acid was studied and experiments showed that a concentration of 2 mM of thioglycolic acid eliminated copper interference up to a concentration of about 1 mg L^{-1}, corresponding to a molar ratio Cu/Ni of 92. A higher concentration of thioglycolic acid led to a slight decrease in the nickel response (increased IF/IF_0 ratio) (Fig. 5b).

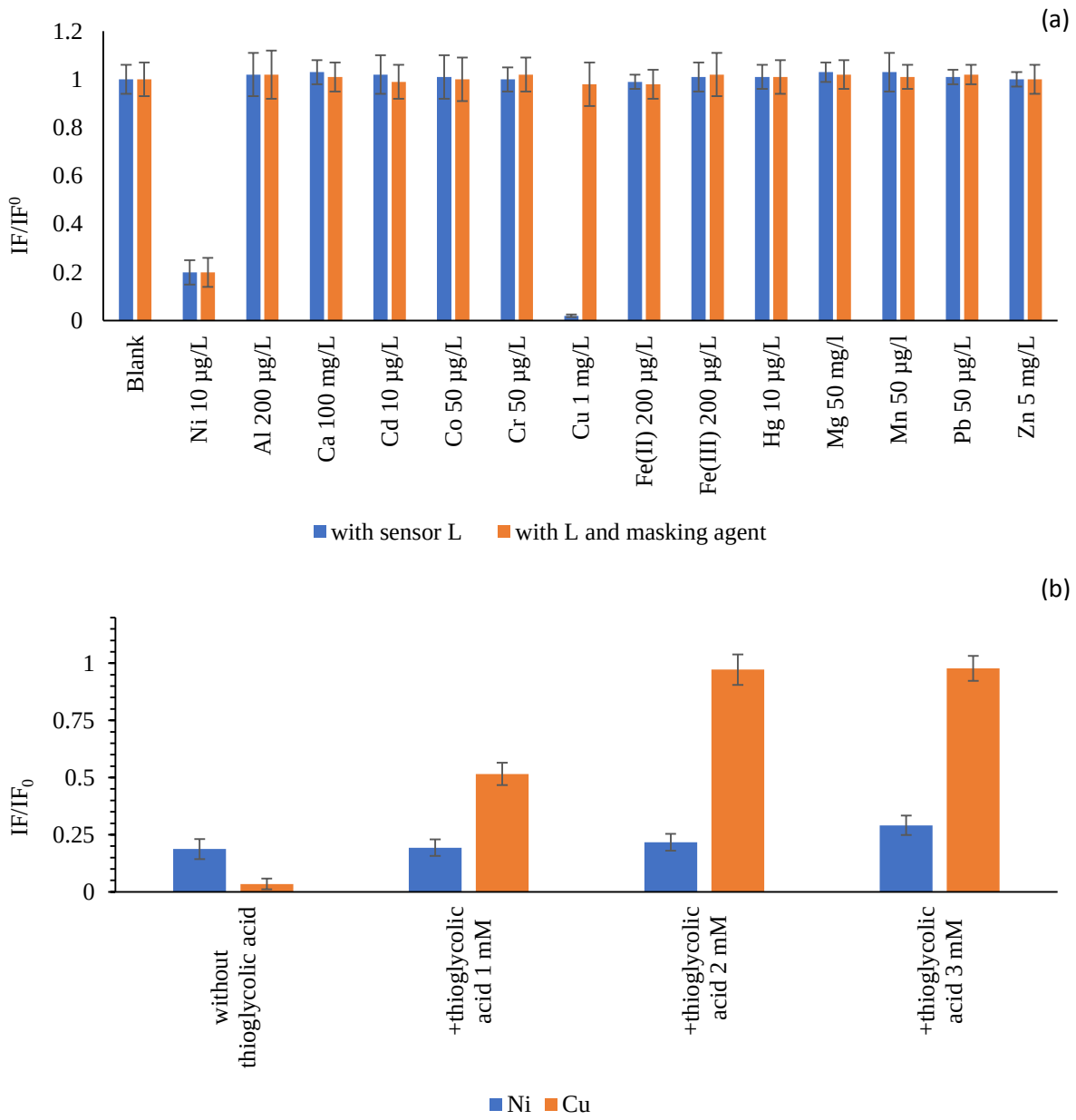

Figure 5: (a) Selectivity study (n=3) with sensor **L** (10 µM) in phosphate buffer (pH=7) towards interfering ions at environmental levels in absence and presence of masking agent (thioglycolic acid 2 mM); (b) Masking effect (n=3) of thioglycolic acid at different concentrations (sensor **L** 10 µM in phosphate buffer (pH=7), Ni 10 µg L^{-1}, Cu 1 mg L^{-1}).

3.4 Analytical features of microplate analytical procedure

A simple microplate analytical procedure with sensor **L** was developed and evaluated using the optimized experimental conditions: 0.1 M buffer phosphate adjusted to a pH value of 7 and 2 mM thioglycolic acid used as masking agent solution. Analytical features of this procedure are presented in Table 2.

Very good linear regression coefficient was obtained with Ni^{2+} standards in the range 1.6 - 40 µg L^{-1} (Fig S4). The limit of quantification (LOQ), defined as the concentration corresponding

to (blank+10σ), was lower than 6 µg L^{-1}, which corresponds to 30% of the parametric value for the quality of water intended for human consumption in Europe for nickel, without the need of a preconcentration step by solid-phase extraction.

The intra-day (8 consecutive repeated measurements on the same day) and inter-day (5 repeated measurements over 5 consecutive days) precision (RSD) of the microplate measurement were evaluated at 2 concentration levels: in the middle of the analytical range, i.e. 20 µg L^{-1}, and at 30% of the parametric value for the quality of water intended for human consumption in Europe for nickel, i.e. 6 µg L^{-1}. The results (Table 2) showed that the developed analytical procedure has the adequate precision recommended by the European legislation for water sanitary control (uncertainty of measurement of 25% at a concentration equals to 30% of the parametric value) with intra-day and inter-day RSD performed at 6 µg L^{-1}, respectively of 7.75 and 8.87%.

By comparing these analytical characteristics with those of methods from the literature (Table 1), this developed analytical procedure seems to be a good compromise between ease of use (the procedure only requires a microplate reader and takes less than a minute), good detection and quantification limits and consideration of interference from metal ions at environmental levels.

Table 2 : Analytical features of the microplate protocol with **L**.

Limit of detection (µg L^{-1})	1.62
Limit of quantification (µg L^{-1})	5.41
Linear working range (µg L^{-1})	1.6 – 40
R^2	0.9972
Intra-day RSD (%)	
20 µg L^{-1} (n=8)	1.84
6 µg L^{-1} (n=8)	7.75
Inter-day RSD (%)	
20 µg L^{-1} (n=5)	2.98
6 µg L^{-1} (n=5)	8.87

3.4 Application to real samples

The certified groundwater material ERM®-CA615 was first used for the validation of the microplate procedure (Table 3), and the t-test for comparison of means showed there were no significant differences, at 95% confidence level.

The optimized microplate procedure was then applied to Ni^{2+} determination in natural waters sampled in Aubagne region (near Marseille city, south-east of France). The samples were UV-

photooxidized at 254 nm for 30 minutes before analysis to degrade natural organic ligands, inorganic ligands, or even anthropogenic organic ligands and to quantify total dissolved nickel. Ni^{2+} was measured in samples in duplicate by the developed microplate procedure and by ICP-MS as reference analytical method. The results are summarized in Table 3. The complete physical-chemical characteristics of the samples are given in Table S2 to give an overview of the possible interferences in the samples measured.

The values obtained by the two methods were consistent despite a slight underestimation by the microplate method. The mean difference between the two methods was -2.94%, (min -0.73%; max -5.4%) but this difference should be put into perspective given the low concentration of nickel in the samples. The results obtained for nickel determination by the proposed microplate method with **L** were compared (paired *t*-test) with the reference method values (ICP-MS). A risk of 1.94% difference was calculated between the two methods.

Table 3 : Nickel determination in natural waters with microplate procedure.

Samples	**Microplate procedure with L ($\mu g\ L^{-1}$)**	**ICP-MS ($\mu g\ L^{-1}$)**
#1 Drilling	4.47 ±0.12	4.62 ±0.009
#2 River	5.41 ±0.23	5.38 ±0.003
#3 Drilling	6.73 ±0.14	6.88 ±0.004
#4 Source	5.71 ±0.17	5.79 ±0.002
#5 Source	8.15 ±0.15	8.21±0.006
	Found value	**Certified value**
Groundwater ERM®-CA615[a]	24.94±0.31	25.3±1.1

[a] Certified mass concentration of cations: As: 9.9 ± 0.7 µg L^{-1}; Cd: 0.106 ± 0.011 µg L^{-1}; Fe: 5.11 ± 0.26 µg L^{-1}; Hg: 0.037 ± 0.004 µg L^{-1}; Mn : 107 ± 5 µg L^{-1}; Pb : 7.1 ± 0.6 µg L^{-1}

3.6 Greenness and sustainability evaluation of the method

The greenness and the sustainability of the method were evaluated using RGB model according to the procedure described in Section 2.7 and were compared to four other methods. The results of the evaluation of the different criteria and the overall score obtained for each method are presented in Figure S5.

For the analytical aspects (red scores), the best scores are obtained by the proposed method and by the methods based on the use of azocalix[4]arene [18] or murexide [21] with red scores of 76.3%, 71.5% and 77.5% respectively. The scores of other methods are penalized either by a lower selectivity (criterion R1 scope of application, corresponding to acceptable molar ratio between Ni and interferents) [8,16], or by a low measurement range [16]. Methods using fluorescence measurement [this work,16,21] or solid phase spectrophotometry (thus integrating a pre-concentration step on the solid phase) [8] have better detection limits than simple

spectrophotometric methods [18] and are therefore capable of measuring concentrations equal to 30% of the parametric value (approximately 6 µg L^{-1}).

Concerning ecological aspects, the proposed method is the most environmentally friendly. Particular attention can be paid to the high score obtained by the developed method compared to other methods in the case of criterion G2 (reagent consumption and waste production), which have been considerably minimized thanks to the adaptation of the analytical method to microplate configuration. The green score of most of the methods is however downgraded by the G1 criterion (toxicity of reagents used) with the use of reagents that are toxic to human health and/or the environment, even more by excluding the chemicals used during the synthesis steps of the chemical probes.

All methods obtain similar blue scores around 80%, except for the one developed by Liu et al [8], based on solid phase spectrophotometry, which obtains a significantly lower score, mainly due to the analysis time (criterion B2) and the large sample volume required (criterion B3).

Finally, the proposed method appears to present best overall score (80.4%), with well-balanced scores between ecological, practical, and analytical performance aspects.

4. Conclusion

This study demonstrated the performance of a simple and rapid microplate analytical method for the determination of dissolved nickel in environmental aqueous samples based on a newly synthesized fluorescent chemosensor **L** (4-[4,5-di(pyridin-2-yl)-1H-imidazol-2-yl]benzoic acid). Optimization of the pH value and the nature of the buffer improved the selectivity of the chemical probe **L**. The limit of quantification obtained (lower than 6 µg L^{-1}) is low enough to apply this method to the analysis of drinking water according to European regulations: for water sanitary control, an analytical method should be capable of measuring concentrations equal to 30% of the parametric value (20 µg L^{-1} for nickel). The optimized microplate procedure has been successfully applied to real natural water samples, demonstrating applicability of our new methodology for Ni^{2+} detection.

Acknowledgements

The work presented in this publication was funded by the French Research Agency ("SMART-3D" project, ANR-18-CE04-0005).

References

[1] T.K. Grimsrud, S.R. Berge, J.I. Martinsen, A. Andersen, Lung cancer incidence among Norwegian nickel-refinery workers 1953–2000, J. Environ. Monit. 5 (2003) 190–197. https://doi.org/10.1039/B211722N

[2] European Food Safety Authority, Opinion of the Scientific Panel on Dietetic Products, Nutrition and Allergies on a request from the Commission related to the Tolerable Upper Intake Level of Nickel, EFSA journal 146 (2005) 1-21. https://doi.org/10.2903/j.efsa.2005.146

[3] D. Chakraborti, Determination of trace metals in natural waters at nanogram per liter levels by electrothermal atomic absorption spectrometry after extraction with sodium diethyldithiocarbamate, Anal. Chim. Acta 196 (1987) 23-31. https://doi.org/10.1016/S0003-2670(00)83066-4

[4] S. Baytak, A.R. Turker, Determination of lead and nickel in environmental samples by flame atomic absorption spectrometry after column solid-phase extraction on Ambersorb-572 with EDTA, J. Hazard. Mater. 129 (2006) 1-3, 130-136. https://doi.org/10.1016/j.jhazmat.2005.08.019

[5] S. Vellaichamy, K. Palanivelu, Preconcentration and separation of copper, nickel and zinc in aqueous samples by flame atomic absorption spectrometry after column solid-phase extraction onto MWCNTs impregnated with D2EHPA-TOPO mixture, J. Hazard. Mater. 185 (2011) 1131-1139. https://doi.org/10.1016/j.jhazmat.2010.10.023

[6] S.L.C. Ferreira, A.C. Spinola Costa, D.S. de Jesus, Derivative spectrophotometric determination of nickel using Br-PADAP, Talanta 43 (1996) 1649-1656. https://doi.org/10.1016/0039-9140(96)01919-4

[7] H. Mizuguchi, R. Ishida, Y. Kouno, T. Tachibana, T. Honda, T. Kijima, Y. Yamamoto, T. Takayanagi, A rapid enrichment technique for the ultratrace determination of nickel in water samples using a nanofiber-composite membrane filter, Anal. Sci. 34 (2018) 907-912. https://doi.org/10.2116/analsci.18P093

[8] Y. Liu, X. Chang, S. Wang, Y. guo, B. Din, S. Meng, Solid-phase spectrophotometric determination of nickel in water and vegetable samples at sub-μg l^{-1} level with o-carboxylphenyldiazoaminoazobenzene loaded XAD-4, Talanta 64 (2004) 160-166. https://doi.org/10.1016/j.talanta.2004.02.002

[9] S. Adewuyi, D.A. Ondigo, R. Zugle, Z. Tshentu, T. Nyokong, N. Torto, A highly selective and sensitive pyridylazo-2-naphthol-poly(acrylic acid) functionalized electrospun nanofiber

fluorescence ‘‘turn-off’’ chemosensory system for Ni^{2+}, Anal. Methods 4 (2012) 1729-1735. https://doi.org/ 10.1039/c2ay25182e

[10] V. Kaur, A.K. Malik, N. Verma, Simultaneous spectrophotometric dtermination of cobalt and nickel by partial least square regression in micellar media, Annali di chimica 97 (2007) 237-249. https://doi.org/10.1002/adic.200790008

[11] Y. Guo, H. Zhao, Y. Han, X. liu, S. Guan, Q. Zhang, X. Bian, Simultaneous spectrophotometric determination of trace copper, nickel, and cobalt ions in water samples using solid phase extraction coupled with partial least squares approaches, Spectroc. Acta A 173 (2017) 532-536. http://dx.doi.org/10.1016/j.saa.2016.10.003

[12] H.-W. Gao, S.-Q. Xia, H.-Y. Wong, J.-F. Zhao, Light-absorption ratio variation approach to determination of nickel (II) in ng/ml level with 1, 5-di(2-hydroxy-5-sulfophenyl)-3-cyanoformazan, Wat. Res. 38 (2004) 1642-1650. http://dx.doi.org/10.1016/j.watres.2003.11.030

[13] M. Dutta, D. Das, Recent developments in fluorescent sensors for trace-level determination of toxic-metal ions, TRAC 32 (2012) 113-132. http://dx.doi.org/10.1016/j.trac.2011.08.010

[14] B. Chowdhury, M. Karar, S. Paul, M. Joshi, A.R. Choudhury, B. Biswas, Salen Type Ligand as a Selective and Sensitive Nickel(II) ion Chemosensor: A Combined Investigation with Experimental and Theoretical Modelling, Sens. Actuator B-Chem 276 (2018) 560-566. https://doi.org/10.1016/j.snb.2018.08.141

[15] C. Wang, J. Fu, K. Yao, K. Xue, K. Xu, X. Pang, Acridine-based fluorescence chemosensors for selective sensing of Fe^{3+} and Ni^{2+} ions, Spectroc. Acta A. 199 (2018) 403-411. https://doi.org/10.1016/j.saa.2018.03.015

[16] M. Liu, Z. Yin, Y. Tan, J. Li, H. Peng, A. Duan, C. Luo, A new acylhydrazine N’-(1,3 dimethylbutylene)-3-hydroxy-naphthohydrazide based fluorescent sensor for the detection of Ni^{2+}, Dyes Pigm. 181 (2020) 108582. https://doi.org/10.1016/j.dyepig.2020.108582

[17] N. Chen, Y. Zhang, H. Liu, H. Ruan, C. Dong, Z. Shen, A. Wu, A Supersensitive Probe for Rapid Colorimetric Detection of Nickel Ion Based on a Sensing Mechanism of Anti-etching, Sustainable Chem. Eng. 4 (2016) 6509-6516. http://dx.doi.org/10.1021/acssuschemeng.6b01326

[18] Q. Ma, H. Ma, M. Su, Z. Wang, L. Nie, S. Liang, Determination of nickel by a new chromogenic azocalix[4]arene, Ana. Chim. Acta 439 (2001) 73-79. https://doi.org/10.1016/S0003-2670(01)01009-1

[19] A.K. Manna, K. Rout, S. Chowdhury, G.K. Patra, A dual-mode highly selective and sensitive Schiff base chemosensor for fluorescent colorimetric detection of Ni^{2+} and colorimetric detection of Cu^{2+}, Photochem. Photobiol. Sci. 18 (2019) 1512-1525. https://doi.org/10.1039/c9pp00114j

[20] M. Dhanushkodi, G.G.V. Kumar, B.K. Balanchandar, S.Sarveswari, S. Gandhi, J. Rajesh, A simple pyrazine based ratiometric fluorescent sensor for Ni^{2+} ion detection, Dyes Pigm. 173 (2020) 107897. https://doi.org/10.1016/j.dyepig.2019.107897

[21] K. Kargosha, M.S. Maleki, J. Azad, Spectrofluorimetric Determination of Nickel (II) with Murexide, J. Fluoresc. 24 (2014) 855-858. https://doi.org/10.1007/s10895-014-1363-6

[22] Y. Bazel, M. Reclo, J. Sandrejova, Using a switchable-hydrophilicity solvent for the extraction−spectrophotometric determination of nickel, J. Anal. Chem. 72 (2017) 1018-1023. http://dx.doi.org/10.1134/S1061934817080032

[23] Q. Yao, Y. Feng, M. Rong, S. He, X. Chen, Determination of nickel(II) via quenching of the fluorescence of boron nitride quantum dots, Microchim. Acta, 184 (2017) 4217-4223. http://dx.doi.org/10.1007/s00604-017-2496-5

[24] Commission Directive (EU) 2015/1787 of 6 October 2015 amending Annexes II and III to Council Directive 98/83/EC on the quality of water intended for human consumption.

[25] K. Nakashima, H. Yamasaki, N. Kuroda, S. Akiyama, Evaluation of lophine derivatives as chemiluminogens by a flow-injection method, Anal. Chim. Acta 303 (1995) 103-107. https://doi.org/10.1016/0003-2670(94)00360-X

[26] N. Kuroda, R. Shimoda, M. Wada, K. Nakashima, Lophine derivatives and analogues as new phenolic enhancers for the luminol–hydrogen peroxide–horseradish peroxidase chemiluminescence system, Anal. Chim. Acta 403 (2000) 131-136. https://doi.org/10.1016/S0003-2670(99)00649-2

[27] D.F. Marino, F. Wolff, J.D. Ingle Jr, Determination of cobalt by lophine chemiluminescence, Anal. Chem. 51 (1979) 2051-2053. https://doi.org/10.1021/ac50048a041

[28] J. Slater, D.M. D'Alessandro, F.R. Keene, P.J. Steel, Metal-metal interactions in dinuclear tuthenium complexes containing bridging 4,5-di(2-pyridyl)imidazolates and related ligands, Dalton Trans. 16 (2006) 1954-1962. https://doi.org/10.1039/B514976M

[29] A.D. Becke, A new mixing of Hartree–Fock and local density- functional theories, J. Chem. Phys. 98 (1993) 1372–1377. https://doi.org/10.1063/1.464304

[30] A.D. Becke, Density- functional thermochemistry. III. The role of exact exchange, J. Chem. Phys. 98 (1993), 5648–5652. https://doi.org/10.1063/1.464913

[31] C. Lee; W. Yang; R.G. Parr, Development of the Colle-Salvetti correlation-energy formula into a functional of the electron density, Phys. Rev. B 37 (1988) 785–789. http://dx.doi.org/10.1103/PhysRevB.37.785

[32] A. Schäfer, H. Horn, R. Ahlrichs, Fully optimized contracted Gaussian basis sets for atoms Li to Kr, J. Chem. Phys. 97 (1992) 2571-2577. https://doi.org/10.1063/1.463096

[33] F. Weigend, R. Ahlrichs, Balanced basis sets of split valence, triple zeta valence and quadruple zeta valence quality for H to Rn: Design and assessment of accuracy, Phys. Chem. Chem. Phys. 7 (2005) 3297-3305. https://doi.org/10.1039/B508541A

[34] A.D. Becke, Density-functional exchange-energy approximation with correct asymptotic behavior, Phys. Rev. A 38 (1988) 3098-3100. http://dx.doi.org/10.1103/PhysRevA.38.3098

[35] S.H. Vosko, L. Wilk, M. Nusair, Accurate spin-dependent electron liquid correlation energies for local spin density calculations: a critical analysis, Can. J. Phys. 58 (1980) 1200-1211. https://doi.org/10.1139/p80-159

[36] J.P. Perdew, Density-functional approximation for the correlation energy of the inhomogeneous electron gas, Phys. Rev. B 33 (1986) 8822-8824. http://dx.doi.org/10.1103/PhysRevB.33.8822. Erratum: J.P. Perdew, Phys Rev B 34 (1986) 7406. http://dx.doi.org/10.1103/PhysRevB.34.7406

[37] S. Grimme, J. Antony, S. Ehrlich and H. Krieg, A consistent and accurate ab initio parametrization of density functional dispersion correction (DFT-D) for the 94 elements H-Pu, J. Chem. Phys. 132 (2010) 154104. https://doi.org/10.1063/1.3382344

[38] TURBOMOLE V7.5 2020, a development of University of Karlsruhe and Forschungszentrum Karlsruhe GmbH, 1989-2007, TURBOMOLE GmbH, since 2007; available from http://www.turbomole.com

[39] R. Ahlrichs, M. Baer, M. Haeser, H. Horn, C. Koelmel, Electronic structure calculations on workstation computers: The program system turbomole, Chem. Phys. Lett. 162 (1989) 165-169. https://doi.org/10.1016/0009-2614(89)85118-8

[40] O. Treutler, R. Ahlrichs, Efficient molecular numerical integration schemes, J. Chem. Phys. 102 (1995) 346-354. https://doi.org/10.1063/1.469408

[41] K. Eichkorn, O. Treutler, H. Öhm, M. Häser, R. Ahlrichs, Auxiliary basis sets to approximate Coulomb potentials (Erratum Chem. Phys. Letters 240 (1995) 283-290), Chem. Phys. Lett. 242 (1995) 652-660. https://doi.org/10.1016/0009-2614(95)00838-U

[42] K. Eichkorn, F. Weigend, O. Treutler, R. Ahlrichs, Auxiliary basis sets for main row atoms and transition metals and their use to approximate Coulomb potentials, Theor. Chem. Acta 97 (1997) 119-124. http://dx.doi.org/10.1007/s002140050244

[43] M. Sierka, A. Hogekamp, R. Ahlrichs, Fast evaluation of the Coulomb potential for electron densities using multipole accelerated resolution of identity approximation, J. Chem. Phys. 118 (2003) 9136-9148. https://doi.org/10.1063/1.1567253

[44] R. Bauernschmitt, M. Häser, O. Treutler, R. Ahlrichs, Calculation of excitation energies within time-dependent density functional theory using auxiliary basis set expansions, Chem. Phys. Lett. 264 (1997) 573-578. https://doi.org/10.1016/S0009-2614(96)01343-7

[45] P. Deglmann, K. May, F. Furche, R. Ahlrichs, Nuclear second analytical derivative calculations using auxiliary basis set expansions, Chem. Phys. Lett. 384 (2004) 103-107. https://doi.org/10.1016/j.cplett.2003.11.080

[46] M.L. Dowling, M.T. Lemaire, Preparation, electrochemical behavior and variable temperature magnetic properties of transition metal complexes containing 2-phenyl-4,5-di-(2-

pyridyl)imidazole, Transition Met. Chem. 39 (2014) 843–848. https://doi.org/10.1007/s11243-014-9866-1

[47] M. E. Casida, Time-dependent density functional response theory for molecules, in Recent advances in density functional methods, Recent Advances in Computational Chemistry, World Scientific, 1 (1995) 155–192. https://doi.org/10.1142/9789812830586_0005.

[48] P.M. Nowak, P. Koscielniak, What color is your method? Adaptation of the RGB additive color model to analytical method evaluation, Anal. Chem. 91 (2019) 10343–10352. https://doi.org/10.1021/acs.analchem.9b01872

[49] P. Koscielniak, P. Mateusz, J. Kozak, M. Wieczorek, Comprehensive assessment of flow analytical methods dedicated to the determination of zinc in water, Molecules 26 (2021) 3914-3925. https://doi.org/10.3390/molecules26133914

[50] N. Fridman, M. Kaftory, Y. Eichen, S. Speiser, Crystal structures and solution spectroscopy of lophine derivatives, J. Mol. Struct. 917 (2009) 101-109. https://doi.org/10.1016/j.molstruc.2008.07.003

[51] J.D. Artiss, S. Vinogradov, B. Zak, Spectrophotometric study of several sensitive reagents for serum iron, Clin. Biochem. 14 (1981) 311-315. http://doi.org/10.1016/s0009-9120(81)91065-1